Hindawi
Shock and Vibration
Volume 2019, Article ID 7149680, 12 pages
https://doi.org/10.1155/2019/7149680

Research Article

An Electro Breakdown Damage Model for Granite and Simulation of Deep Drilling by High-Voltage Electropulse Boring

Changping Li[1,2] **Longchen Duan**[3] **Songcheng Tan**[3] **Victor Chikhotkin**[3] **and Xiaohui Wang**[2]

[1]*School of Automation, China University of Geosciences, Wuhan 430074, China*
[2]*School of Mechanical Engineering and Electronic Information, China University of Geosciences, Wuhan 430074, China*
[3]*Faculty of Engineering, China University of Geosciences, Wuhan 430074, China*

Correspondence should be addressed to Longchen Duan; duanlongchencug@163.com

Received 15 August 2019; Revised 16 October 2019; Accepted 15 November 2019; Published 29 November 2019

Academic Editor: Mario Terzo

Electropulse rock breaking has wide application prospects in hard rock drilling and ore breaking. At present, there are no suitable physical mathematical models that describe electropulse boring (EPB) processes under confining pressures. In this paper, a high-voltage electropulse breakdown damage model is established for granite, which includes three submodels. It considers electric field distortions inside the rock, and an electric field distribution coefficient is introduced in the electro-breakdown model. A shock-wave model is also constructed and solved. To simulate the heterogeneity of rocks, EPB rock breaking in deep environments is simulated using the two-dimensional Particle Flow Code (PFC2D) program. The solved shock wave is loaded into the model, and confining pressure is applied by the particle servo method. An artificial viscous boundary is used in the numerical simulation model. Using this approach, a complete numerical simulation of electropulse granite breaking is achieved. Breakdown strength and the influences of physical and mechanical parameters on it are also obtained. Time-varying waveforms of electrical parameters are obtained, and the effect of confining pressure on EPB is also described.

1. Introduction

In the future development of crude oil, natural gas, and geothermal wells, deep and ultradeep wells will need to be drilled [1–4]. EPB is a recently developed rock breaking technology [5, 6]. Compared with other rock breaking methods, it has the advantages of controllable energy levels, no pollution, no flying rock particles, and low cost. In the process of EPB, high voltages with short rising edges and high electrical currents are required; however, there is a problematic time delay between the occurrence of the peak voltage and peak current [7, 8]. He et al. [9] developed pulse generators with both voltage source and current source based on the characteristics of the peak voltage-peak current delay found in the process of electropulse rock breaking.

There are various macro-sized and micro-sized defects in rock which greatly influence the electric field distribution in the rock and the rock breaking efficiency [10–12]. The drilling environments encountered during EPB at great depths are complex. Currently, there are no models of rock fragmentation during EPB in deep wells [3, 13]. In their research into high-voltage electro-pulse rock breaking models, Andres et al. [14] and Li et al. [15] established models of electric field distributions in composite media. The effects of electro-pulse rock breaking were obtained indirectly based on electric field distributions in rock. Zhang [16] built a model of rock fragmentation by plasma channel based on the principles of momentum transfer. Consistent with classical explosion theory, rock was regarded as a homogeneous, isotropic, and incompressible fluid in the model. Burkin et al. [17, 18] proposed a dynamic model of electrical explosions. The model assumed that the material is continuous during the time interval considered. Parameters such as voltage, current, and the radial force and tangential force waveform were obtained by numerical simulation. Kuznetsova et al. [19, 20] built an electroexplosion model

based on the plastic-elastic deformation of a solid medium and the dynamics of a liquid medium. Theoretical and experimental investigations of electro-discharge destruction were carried out. The validity and effectiveness of the electro-explosion model were demonstrated, and the model was used to predict voltage and current waveforms during EPB. However, the pressure of the plasma channel after electrical breakdown generally ranged from hundreds of MPa to several GPa, while the volume compression modulus or radial compression modulus of the rock was generally tens to hundreds of GPa. Hence, the physical process of EPB could not be well simulated and explained. Cho et al. [21–23] adopted a quasi-static multicrack model in ANSYS to simulate the rock fracture process by loading the known pressure waveform. In order to verify the influence of formation pressure on electro-pulse rock breaking, a high-voltage pulse discharge breaking experiment was carried out by Sun et al. [24] with a maximum confining pressure of 35 MPa (corresponding to a drilling depth of 3000 m). It was demonstrated that higher pulse voltages are needed to break rock and the breaking height decreases with increases in confining pressure. However, the mechanism of this effect remains unknown.

According to the characteristics of rock's nonuniformity, pores, and electric field distortions, an electro-breakdown model was established based on the theory of breakdown weak points and the cylindrical channel model. A proportional coefficient of the electric field distribution was incorporated into the model. The breakdown electric field strength of granite was obtained under specific physical parameters, and the effects of the rock's physical parameters on it were obtained. An equivalent discharge circuit of electro-pulse rock breaking was established. The waveforms of voltage, current, and shock waves that occur in the process of EPB with specific electrical parameters were solved based on a shock-wave model. The shock wave calculated from the electric parameters was loaded into the numerical simulation model of EPB rock breaking under confining pressure, and then, the rock breaking effects of electro-pulses at various depths were simulated. The effect of EPB rock breaking in deep environments was simulated by PFC2D, which can effectively simulate the mechanical problems of discontinuous media, such as fracture and separation. An artificial viscous boundary was loaded into the numerical simulation model to make it more accurate. By establishing an electrical breakdown damage model, we can simulate the complete process of electro-pulse rock breaking, from electrical breakdown to shock wave generation and, finally, to rock cracking or breaking.

2. Principles of High-Voltage Pulsed Rock Breaking

There are two types of rock breaking by high-voltage pulse discharge: hydroelectric and electro-pulse, of which the latter is more efficient [25–28]. When a high-voltage pulse is applied, a high-voltage electric field is generated in the insulating medium (low-conductivity water or oil) and rock, as shown in Figure 1. When the applied high-voltage short

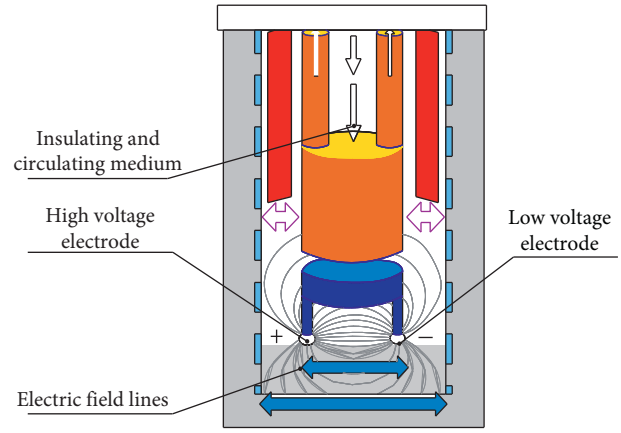

Figure 1: Schematic representation of electro-pulse rock breaking.

pulse rises to its peak value within 500 ns [29–31] and the high- and low-voltage electrodes come into contact with the rock, the breakdown field strength of the rock is less than that of the liquid medium. The rock is broken down by the high-voltage electric field first, and a plasma channel is generated. Then, the stored energy in the power supply is injected into the plasma channel. As the plasma channel expands, stress is generated. When this stress exceeds the rock strength, the rock will break.

A schematic representation of the high-voltage EPB rock-breaking system is shown in Figure 2. The main components are the EPB tool, a drilling tool putting system, a drilling fluid purification and pumping device, and a low-conductivity liquid medium. In the process of EPB rock breaking, the electrode comes into contact with the bottom of the drill hole without rotation and frequent lifting. Mechanical wear of the electrode bit is small, and continuous drilling can be realized with high drilling efficiency.

3. Establishment of Electro-Breakdown Damage Model by High-Voltage Electro-Pulse

The EPB process can be divided into three phases: (1) electro-breakdown, (2) energy injection into the plasma channel, and (3) shock-wave fracturing [32, 33]. These phases can be simulated by a high-voltage electro-pulse breakdown model, shock wave model, and numerical simulation model, respectively. A structural composition and information flow diagram of an electro-breakdown damage model is shown in Figure 3. The electric field strength and mechanism of granite influence estimated by the breakdown model can provide a basis for determining the voltage source and electrode spacing of the electrode bit. After the electro-breakdown of rock, a plasma channel is generated. High current can be obtained by switching to the current source of the power supply and injecting it into the plasma channel.

Shock waves are generated in the plasma channel. Waveforms of voltage, shock waves, and associated parameters can be calculated by the shock-wave model. The shock-wave waveform can be loaded into the numerical simulation model. Confining pressure and a viscous

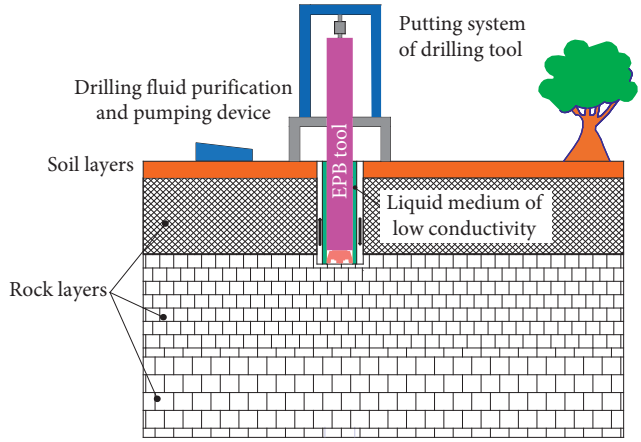

Figure 2: Structural sketch of an EPB rock-breaking system.

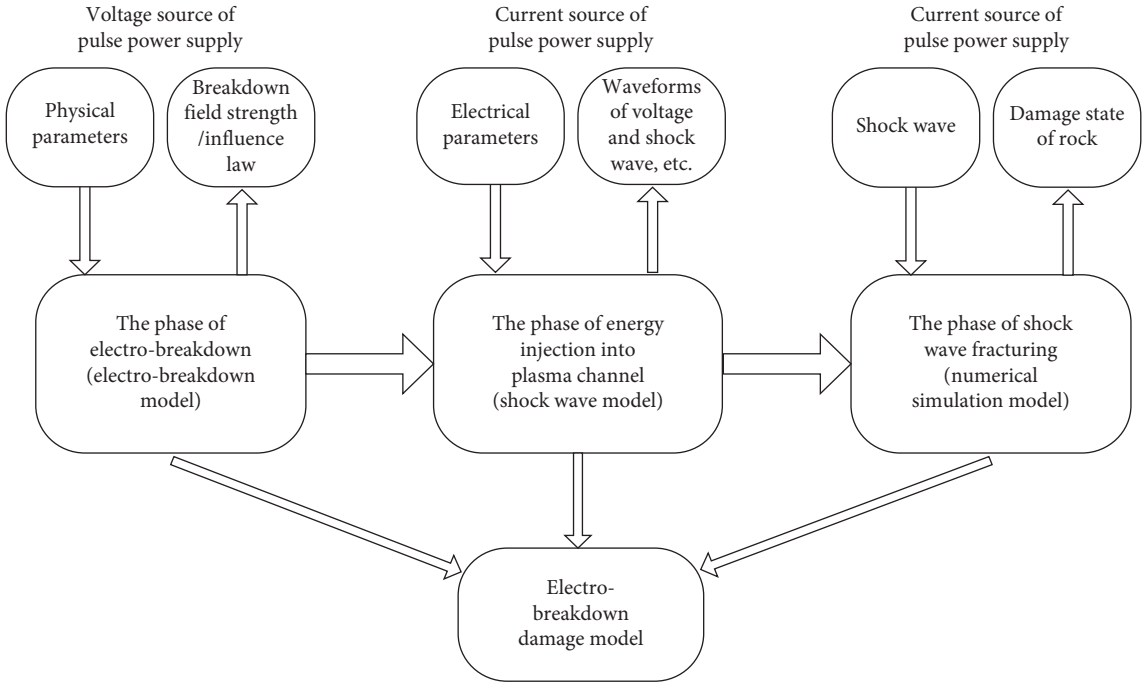

Figure 3: Structural composition and information flow diagram of the electro-breakdown damage model.

boundary were set in the model, allowing simulations under different confining pressures to be carried out.

3.1. Establishment of the Electro-Breakdown Model. In an electrostatic field environment, the breakdown type of rock is electro-breakdown. According to the theory whereby breakdown occurs at weak points [32], the breakdown of solid dielectrics begins at weak points such as cracks or holes. The Kratal cylindrical channel model was used as the plasma channel model of electro breakdown in this paper [33]. As shown in Figure 4, l_{td} is the length of the plasma channel, V_{td} is the volume of the plasma channel, and r is its radius.

In the electrostatic field, the plasma channel contains electrostatic and electromechanical energy [34]. The electrostatic energy W_{es} can be expressed as

$$W_{es} = \frac{1}{2}\mathbf{D}\mathbf{E}v_{td}, \tag{1}$$

where $v_{td} = \pi r^2 l_{td}$, r is the radius of the plasma channel (=10 μm) [17], $\mathbf{E}$ is the electric field strength vector of the hole at the end of the plasma channel, $\mathbf{D}$ is the displacement vector where $\mathbf{D} = \mathbf{E}\,\varepsilon_0\varepsilon_r$, ε_0 is the vacuum dielectric constant (=8.85×10^{-12} F/m), and ε_r is the relative dielectric constant of granite (=8.3) [15]. The electromechanical energy W_{em} in the channel can be expressed as

$$W_{em} = \frac{1}{2}\boldsymbol{\sigma}\boldsymbol{\gamma}\pi r^2 l_{td}. \tag{2}$$

Here, $\boldsymbol{\sigma}$ is the Maxwell stress, which can be expressed as $\boldsymbol{\sigma} = \varepsilon_0\varepsilon_r\mathbf{E}^2/2$, and $\boldsymbol{\gamma}$ is the strain, where $\boldsymbol{\gamma} = \boldsymbol{\sigma}/E_t$. E_t is the elastic modulus of granite (=4.8×10^4 MPa) [15]. The total

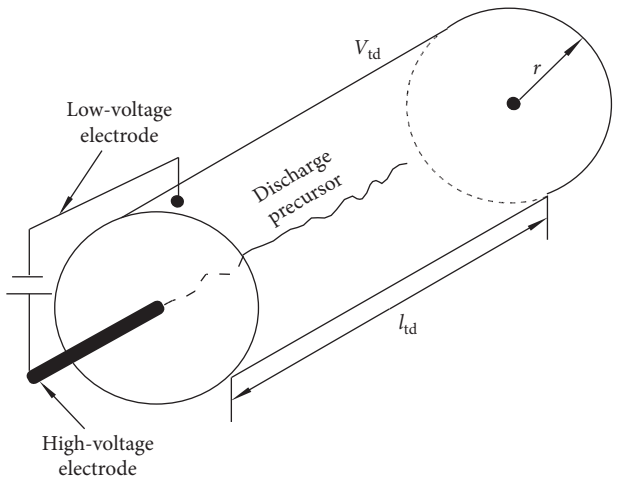

Figure 4: Cylindrical plasma channel model.

energy W_{et} of the plasma channel under the electrostatic field is the sum of the electrostatic energy W_{es} and the electromechanical energy W_{em} in the channel:

$$W_{et} = \left(\frac{\varepsilon_0^2\varepsilon_r^2\mathbf{E}^4}{8E_t} + \frac{\varepsilon_0\varepsilon_r\mathbf{E}^2}{2}\right)\pi r^2 l_{td}. \quad (3)$$

With increases in the applied electric field and expansion of the plasma channel, it is necessary to overcome the surface energy of the granite, W_{ec}. When the total energy inside the granite holes is $\geq W_{ec}$, the plasma channel expands until the high- and low-voltage electrodes are connected. Then, electro-breakdown of granite occurs:

$$W_{ec} = 2G_{ec}\pi r l_{td}, \quad (4)$$

$$W_{et} \geq W_{ec}. \quad (5)$$

Here, G_{ec} is the surface free energy of granite per unit surface area (=48.8 mJ/m^2) [35]. The breakdown electric field strength E_{0c} in the granite can be obtained using formulas (3)–(5) as follows:

$$E_{0c} = \left(\frac{2}{r\varepsilon_0\varepsilon_r}\left(\sqrt{r^2E_t^2 + 4G_{ec}rE_t} - rE_t\right)\right)^{1/2}. \quad (6)$$

Under the action of the external electric field, an induced charge is generated in the end hole of the plasma channel, where free charge exists. The two parts of the charges change the electric field intensity around the hole. The relationship between the external electric field intensity E_c and the electric field intensity inside the hole E_{0c} is as follows [36]:

$$E_{0c} = hE_c, \quad (7)$$

where h is the proportional coefficient of the electric field distribution, which can be expressed as

$$h = \frac{k\varepsilon_r}{1 + (k-1)\varepsilon_r}, \quad (8)$$

where k is a dimensionless constant and related to the plasma channel size and orientation. Assuming that the inner hole of the granite is an ordinary sphere, $k = 3$ [36]. It can be concluded that the electric field strength E_c required for the electro-breakdown of granite can be expressed as follows:

$$E_c = \frac{1 + 2\varepsilon_r}{3\varepsilon_r}\left(\frac{2}{r\varepsilon_0\varepsilon_r}\left(\sqrt{r^2E_t^2 + 4G_{ec}rE_t} - rE_t\right)\right)^{1/2}. \quad (9)$$

3.2. Establishment of a Shock-Wave Model of Electro-Pulse Rock Breaking. In the process of rock breaking by a high-voltage pulsed power supply, there exists electrical-circuit resistance and inductive inductance. The electrical-circuit resistance comprises the resistances of the connecting wires and capacitors, while the inductive inductance comprises the inductances generated in the connecting wires and discharge channels. An equivalent circuit diagram of high-voltage pulsed granite breaking is shown in Figure 5.

Considering granite as the fragmentation object, the electrical impedance of granite extends from the electrical insulation to the breakdown point at which the plasma channel is generated and it has a functional relationship with the discharge time and current. The plasma channel impedance model used here adopts the Weizel–Rompe model [32], and the impedance can be expressed in the form of a current integral, as follows:

$$R_{td}(t) = K_{td} \times l_{td}\left(\int_0^t i^2(t)\mathrm{d}t\right)^{-1/2}. \quad (10)$$

In formula (10), K_{td} is the resistance coefficient (=611 V·S$^{1/2}$/m) [33] and l_{td} is the length of the plasma channel (assumed to be equal to the distance between the electrodes). The electrode bit of the EPB tool is arranged with a coaxial cylindrical electrode. The distance between the electrodes is 10 mm, and i is the discharge circuit current. According to the equivalent circuit shown in Figure 5 and the Kirchhoff loop equation, we conclude that

$$L_{in} \times \frac{\mathrm{d}i}{\mathrm{d}t} + (R_z + R_{td}) \times i(t) + U_c(t) = 0. \quad (11)$$

Here, R_z is the resistance of the electric circuit and (=1 Ω), L_{in} is the inductance (=5 μH) [17], and U_c is the instantaneous voltage of the capacitor. The energy storage capacitance C is

$$C\frac{\mathrm{d}U_c(t)}{\mathrm{d}t} = i(t). \quad (12)$$

Formulas (10) and (12) were substituted into formula (11), and the two sides of the equation were differentiated, resulting in

$$\frac{\mathrm{d}^2i(t)}{\mathrm{d}t^2} + \left[\frac{R_z}{L_{in}} + \frac{K_{td}l_{td}}{L_{in}}\left(\int_0^t i^2(t)\mathrm{d}t\right)^{-1/2}\right]\frac{\mathrm{d}i(t)}{\mathrm{d}t} - \frac{K_{td}l_{td}}{2L_{in}}\left(\int_0^t i^2(t)\mathrm{d}t\right)^{-3/2} \times i^3(t) + \frac{1}{L_{in}C} \times i(t) = 0, \quad (13)$$

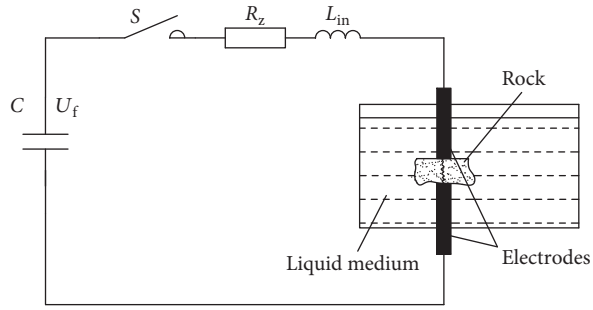

FIGURE 5: Equivalent circuit of high-voltage pulsed granite breaking: C = total equivalent capacitance; S = discharge switch; R_z = circuit resistance; L_{in} = inductive inductance; and R_{td} = plasma channel resistance.

where C is the equivalent capacitance power supply. Its value refers to the current source of the pulse generators that He et al. [9] developed. The value of C is 22 μF, and the charge voltage is 10 kV. According to the equivalent circuit, the energy of the plasma channel can be expressed as follows:

$$W_{td}(t) = \int_0^t i^2(t) \times R_{td} dt. \tag{14}$$

According to the principle of energy balance, the energy from the high-voltage power supply is injected into the plasma channel, where it is converted into heat- and shock-wave energy during the expansion of the plasma channel. The energy conservation equation is as follows [16]:

$$\frac{dW_{td}}{dt} = \frac{P \times dV_{td}}{dt} + \frac{1}{\gamma - 1} \frac{d(PV_{td})}{dt}. \tag{15}$$

Here, γ refers to the equal entropy index. The distribution of the shock wave and heat energies in the plasma channel is determined using the equal entropy index. For condensed materials, its value ranges from 1.05 to 1.25, and the value used in this model was 1.1 [16]. P is the shock-wave pressure of the plasma channel. For rock solids, the plasma channel generated by electro-breakdown in a solid can be regarded as an expanding cylindrical piston. According to the cylindrical plasma channel model and Rankine–Hugoniot's relationship of it to the shock front [37], the relationship between the plasma channel expansion volume and the energy injected into the plasma channel can be expressed as follows:

$$\frac{dV_{td}}{dt} = \left(\frac{\sqrt{7}\,\alpha^{1/14}}{3\sqrt{\rho_0}}\right) \times \left[\left(\frac{W_{td}}{V_{td}} \times \frac{\gamma - 1}{\gamma} + \beta\right)^{3/7} - \beta^{3/7}\right] \times \left(\sqrt{\frac{V_{td}}{\pi l_{td}}} \times 2\pi l_{td}\right). \tag{16}$$

Here, α and β are the shock coefficients (3.001×10^8 Pa and 3.0×10^8 Pa, respectively) [37] and ρ_0 is the density of granite (2660 kg/m^3). By using a differential equation with a variable order and Euler's method for cooperative solving of formulas (13)–(16), we obtain the variations in discharge voltage, discharge current, energy injected into the plasma channel, shock-wave pressure, and plasma channel radius with time.

3.3. Establishment of a Numerical Simulation Model for EPB Rock Breaking under Confining Pressure. In deep and ultra-deep wells, EPB is influenced by many factors, such as the high temperatures and pressures found in such wells. The confining pressure of granite in deep and ultradeep wells has a considerable influence on the efficiency and energy losses of EPB rock breaking [24]. The parallel bond model, the most commonly-used particle contact constitutive model in PFC2D, was used to simulate the physical and mechanical states of the rock. The size models of the circular and rectangular domains, as shown in Figure 6, were used to simulate and analyze the breaking state of the granite surface and interior, respectively.

The shock-wave pressure calculated by the shock-wave model was loaded into the plasma channel pore area of the surface and internal damage models. The shock-wave pressure was transformed into the normal and tangential forces of the spherical particles in the area of the plasma channel pore and iterated continuously until the set time step was reached or the coordinate sphere exceeded the plasma channel pore area:

$$F_n = \frac{P \times (\pi\, d)}{\text{num}} \sin\,\theta, \qquad F_s = \frac{P \times (\pi\, d)}{\text{num}} \cos\,\theta. \tag{17}$$

Here, F_n and F_s represent the normal and tangential forces, respectively, d is the diameter of the plasma channel pore area (=3 mm), and num represents the number of spheres within the plasma channel pore, and θ is the angle between the central connection of sphere particle and the plasma channel hole with the horizontal direction.

A dynamic boundary [38] should be set in the numerical simulation model to absorb the shock wave and prevent it from reentering the model due to boundary reflection and superposition, which could cause simulation error. A reaction force was applied for simulation of the viscous artificial boundary in this paper. By traversing the particles in contact with the boundary wall and giving the boundary particles an opposite force, the process of absorbing seismic waves can be simulated. Considering that the PFC boundary is uneven, a boundary adjustment coefficient is added to more accurately solve the viscous boundary conditions. Based on the continuum theory [39], the equation of the viscous boundary was obtained as

$$\sum F_b = \alpha_b D C_b \rho_0 \frac{du_b}{dt}. \tag{18}$$

Here, the sum of the contact forces, $\sum F_b$, on the artificial boundary is the sum of the component forces on the boundary. D is the particle unit diameter, and α_b is the influence factor of the two-dimensional particle size. In order to achieve the best absorption effect, the particle size influence factor can be adjusted continuously. The value used here is 0.05 [40]. C_b is the wave velocity in the continuous medium (=4535 m/s) [40], ρ_0 is the density of the

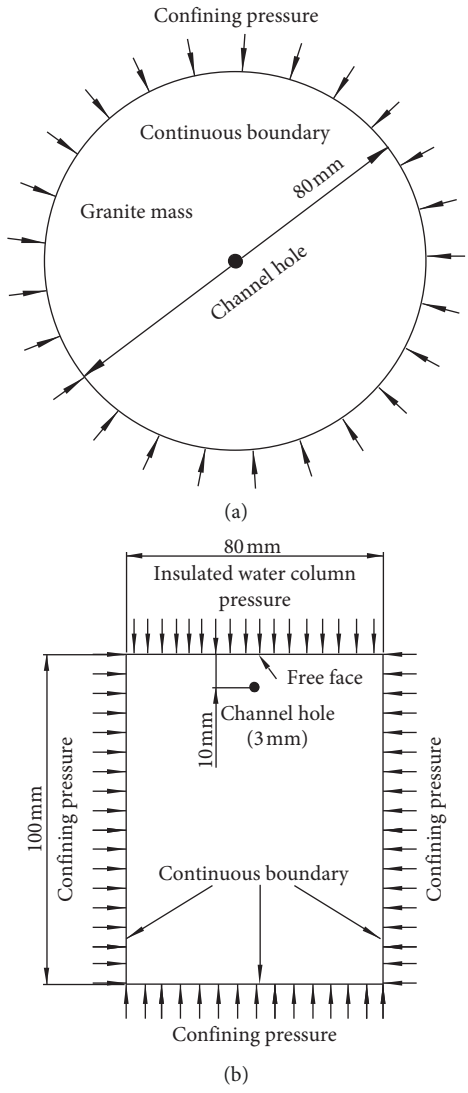

Figure 6: Models of EPB in granite under confining pressure: (a) Surface damage and (b) internal damage.

propagation medium (granite), and u_b is the vibration displacement of the boundary particle.

In PFC2D, stress could not be directly applied to the wall element. In the model, the servo method [41] was used to control the movement of the rigid wall to meet the requirements of the confining pressure conditions. The confining pressure was applied in the rigid servo mode in the granular discrete element model. A constant confining pressure was applied to the left, right, and lower walls of the granular model, and an insulated water column pressure was applied to the top in the rectangular domain. In the circular domain model of the granite surface, firstly, confining pressure was applied to the rectangular domain in the rigid servo mode, and then the spherical particles outside the required circle were removed so that the confining pressure could be applied in the flexible particle servo mode. The confining pressure of deep rock is the product of the lateral pressure coefficient, granite density, gravitational acceleration, and the buried depth of the granite [42]. The confining pressures of deep granite at 3000 m, 2000 m, and 1000 m are approximately 34 MPa, 23 MPa, and 12 MPa, respectively. At the same time, the insulated water column pressures of deep granite at 3000 m, 2000 m, and 1000 m can be calculated as approximately 30 MPa, 20 MPa, and 10 MPa, respectively. The minimum radius of the spherical particles was 0.4 mm, and the maximum radius was 0.6 mm. The plasma channel distance in the electro-pulse-broken granite was 10 mm from the free surface. The microscopic parameters of the granite particle model used during the simulation are shown in Table 1.

4. Results and Discussion

4.1. Numerical Calculation of Electro-Pulse Breakdown. According to the revised electro-breakdown field strength formula and the physical and mechanical parameters of granite, the electro-breakdown field strength of granite under normal temperature and pressure was calculated as 115.2 kV/cm. This value has the same order of magnitude as the experimental results of Vazhov et al. [44] and Lisitsyn et al. [45]. The tested electro-breakdown field strength of granite was 100–150 kV/cm. When the ratio of the EPB voltage to the distance between the high- and low-voltage electrodes in the electrode bit was larger than the electro-breakdown field strength of the granite, then electro-breakdown can be realized by a single discharge. The maximum output voltage of the voltage source designed by He et al. [9] was 120 kV. Hence, the breakdown of the primary discharge of granite can be realized without considering the energy leakage when the distance between the electrodes is 10 mm. At the same time, the cumulative effect of pulse voltage on granite can be used to achieve electro-breakdown, which can reduce the electric field intensity requirements.

The interior of the earth is a high-temperature environment. The physical and mechanical properties of rocks are highly dependent on temperature. Temperature influences the density, porosity, *P*-wave velocity, elastic modulus, and cohesion of granite. The electro-breakdown field strength of granite can be calculated by the electro-pulse breakdown model when the physical and mechanical parameters of deep rock are known. The model of electro-pulse breakdown of granite shows that the electro-breakdown field strength of granite is affected by the relative dielectric constant, the elastic modulus of granite, and other parameters. Using this model, the electro-breakdown field strength of granite can be calculated for different values of the relative dielectric constant, elastic modulus, and other parameters. The relative dielectric constant of granite varied from 8.3 to 15.3, in intervals of 0.5. The breakdown field strength of granite at different dielectric constants was obtained as shown in Figure 7(a). It can be concluded that the electro-breakdown field strength decreased with increases in the relative dielectric constant of granite. The main reason is that the surface energy that the granite needs to overcome remains unchanged and the required electro-breakdown field strength decreases with increases in the relative dielectric constant of granite. The elastic modulus of granite ranged from 48 GPa to 188 GPa, in intervals of 10 GPa. The electro-breakdown field strength

Table 1: Microscopic parameters of the granite particle model [43].

Parameter units	Value	Parameter maturity	Value	Parameter	Value
Particle density (kg/m^3)	2660	Intergranular contact modulus (GPa)	6.53	Tensile strength (MPa)	15
Cohesion (MPa)	20	Friction angle (°)	45	Friction coefficient of particles	0.5
Porosity	0.2	Normal-shear stiffness ratio	2.5	Parallel-link radius coefficient	1

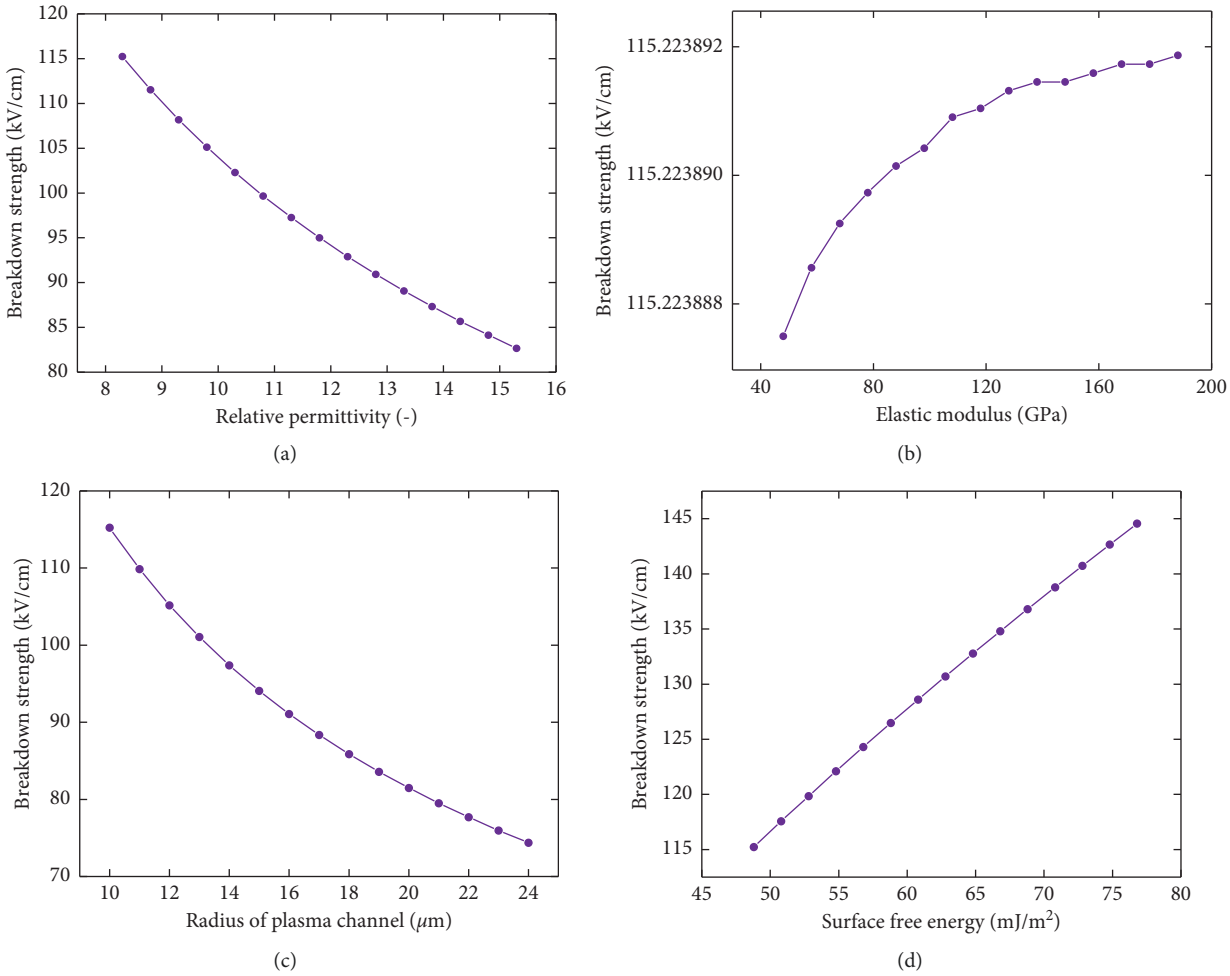

Figure 7: Relationships between electro-breakdown field strength and (a) relative dielectric constant, (b) elastic modulus, (c) plasma channel radius, and (d) surface free energy per unit surface area.

at different elastic moduli can be obtained as shown in Figure 7(b) when the other parameters of the model are held constant. With increases in the elastic modulus of granite, the electro-breakdown field strength increases, but the effect of the elastic modulus on the electro-breakdown field strength is small. The granite plasma channel radius ranged from 10 μm to 24 μm, in intervals of 1 μm. The electro-breakdown field strengths at different plasma channel radii are shown in Figure 7(c), with other model parameters held constant. It is concluded that the electro-breakdown field strength decreases with increases in the plasma channel radius. The surface free energy of granite per unit surface area ranged from 48.8 mJ/m^2 to 76.8 mJ/m^2, at intervals of 2 mJ/m^2. The electro-breakdown field strength at different surface free energies can be obtained as shown in Figure 7(d) (with other model parameters held constant). It is concluded that the breakdown electric field strength of granite increases linearly with increases in surface free energy.

4.2. Numerical Calculation of Shock Waves Caused by Electro-Pulse Rock Breaking. Waveforms of the voltage, energy, current, power, radius, and shock wave of the plasma channel can each be solved according to the electrical parameters of the pulsed power supply as reported by He et al. [9], the shock-wave model of electro-pulse rock breaking. These waveforms are as shown in Figure 8.

The electro-pulse rock breaking conducted in this study can be divided into three stages. The first stage had a rapid rise in

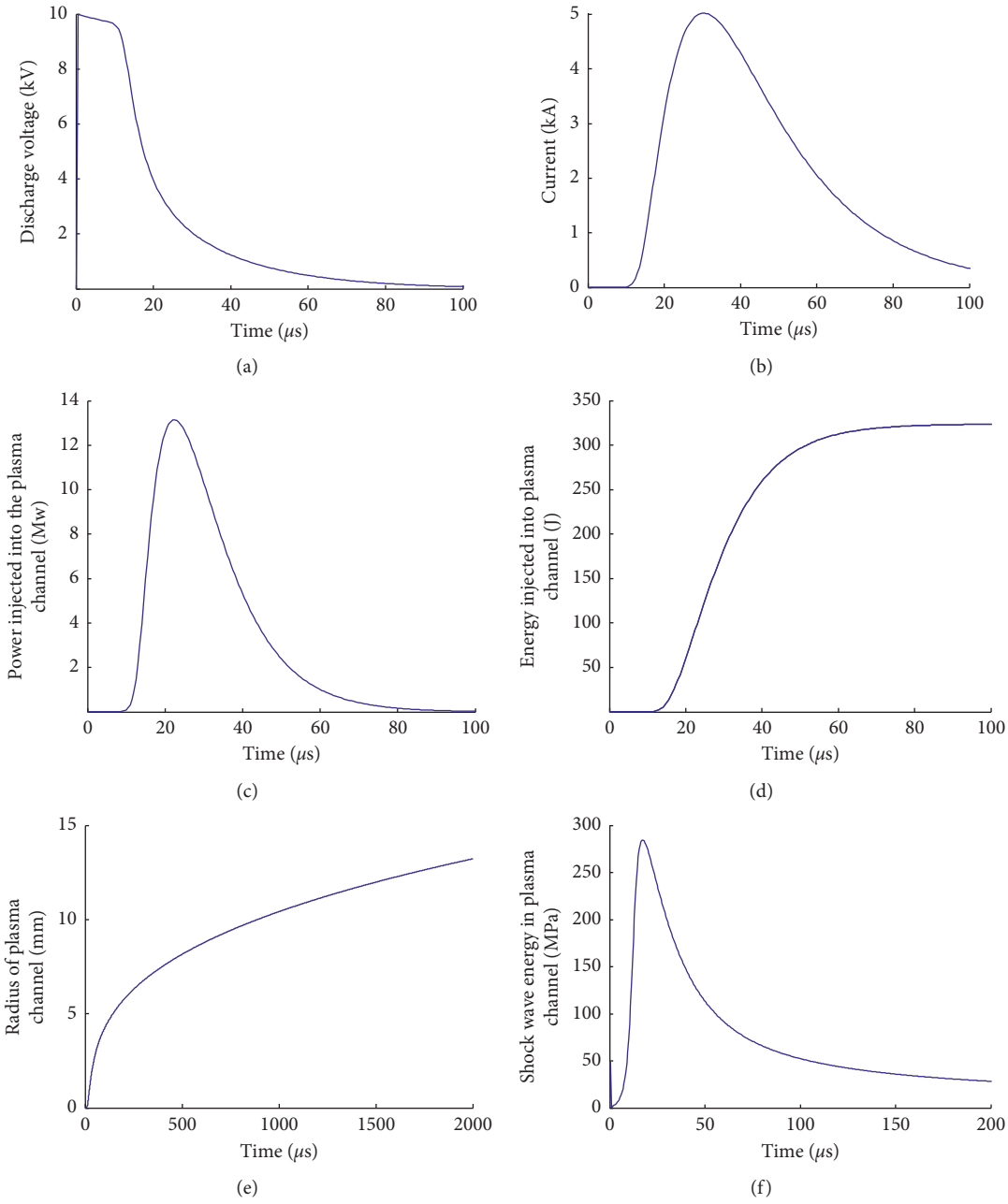

Figure 8: Plasma channel waveforms: (a) Voltage; (b) current; (c) power; (d) energy; (e) radius; and (f) shock wave.

high, short-pulse voltage. The voltage rose to a peak of 10 kV within 0.5 μs. The decrease in peak voltage was small and occurred within 15 μs. The second stage featured a rapid decline in the voltage of the high-voltage electrode and a rapid increase in current. The peak current reached 5 kA, and the peak power reached 13.1 MW. In the third stage, the injected energy expanded the plasma channel. At this time, the current, voltage, and instantaneous power decreased rapidly, and the shock wave energy was converted into internal energy, kinetic energy, and the wave energy reflected at the solid-liquid interface of the granite. In this stage, the radius of the plasma channel increased continuously as it began to expand after being heated. When the stress exceeded the stress intensity of the rock, the rock broke. Eventually, the energy injected into the plasma channel was about 323.7 J. The peak value of the shock wave generated by the plasma channel's expansion was 284 MPa. This fragmentation process is consistent with the observations conducted using CT scanning and the high-speed camera [22].

4.3. Numerical Simulation of EPB Rock Breaking under Confining Pressure. The shock wave calculated by the shock-wave model can be loaded into the numerical model of electro-pulse rock breaking under confining pressure. Using oil or pure water insulation and ignoring electrode energy

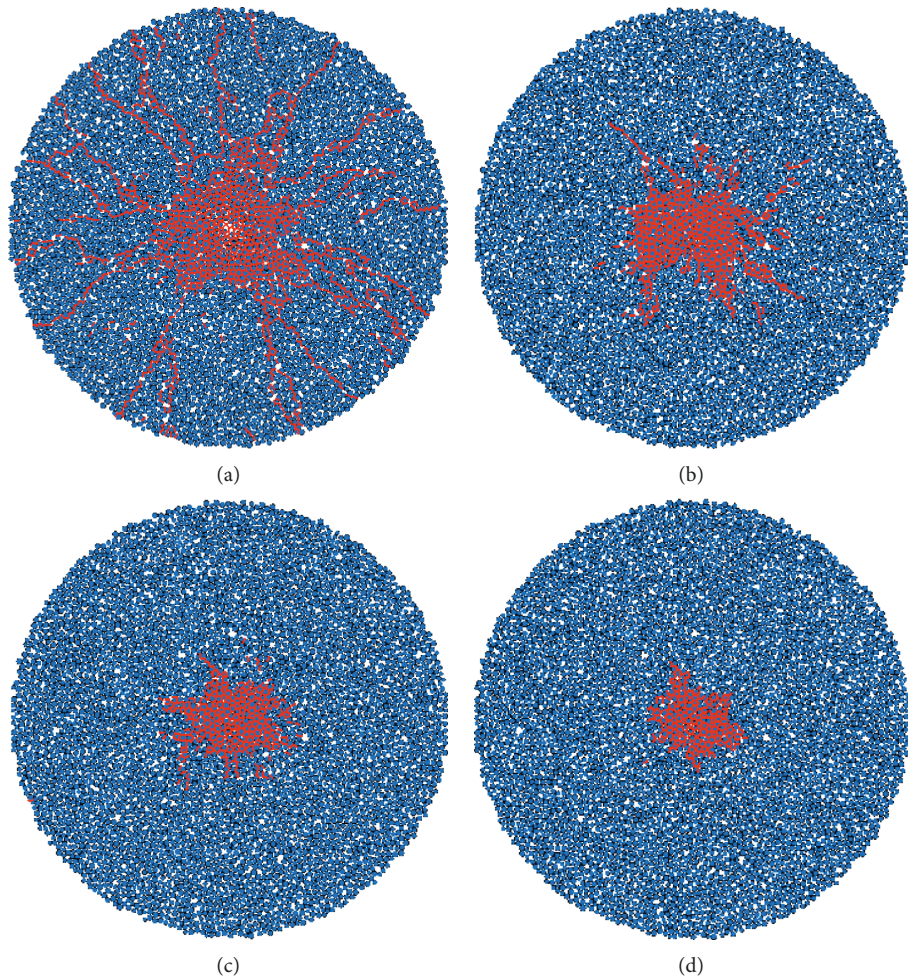

Figure 9: Breaking state of an electropulse at 100 μs on the surface of granite at confining pressures of (a) 0 MPa; (b) 12 MPa; (c) 23 MPa; and (d) 34 MPa.

leakage, electro-pulse rock breaking under confining pressure was simulated and analyzed.

Granite drilling in deep and ultradeep wells is affected by high temperatures and confining pressures and other complex environmental factors that affect electro-pulse rock breaking efficiency. As shown in Figure 9, confining pressures of 0 MPa, 12 MPa, 23 MPa, and 34 MPa were used to simulate EPB drilling at depths of 0 km, 1 km, 2 km, and 3 km, respectively. Moreover, the electro-pulse breaking state of surface granite at 100 μs was simulated by a loading shock wave calculated by the electro-pulse shock wave model. The radius of the crushing zone changed little with increases in confining pressure. The figure shows that different confining pressure loadings had little influence on the blasting crushing zone, although cracks decreased in length and number. That is, confining pressure inhibited the propagation of cracks. This phenomenon can be attributed to the fact that the strength, peak strain, and compressive modulus of rock increase with confining pressure. Then, the number and length of cracks decrease accordingly in rock breaking by a shock wave caused by an electropulse.

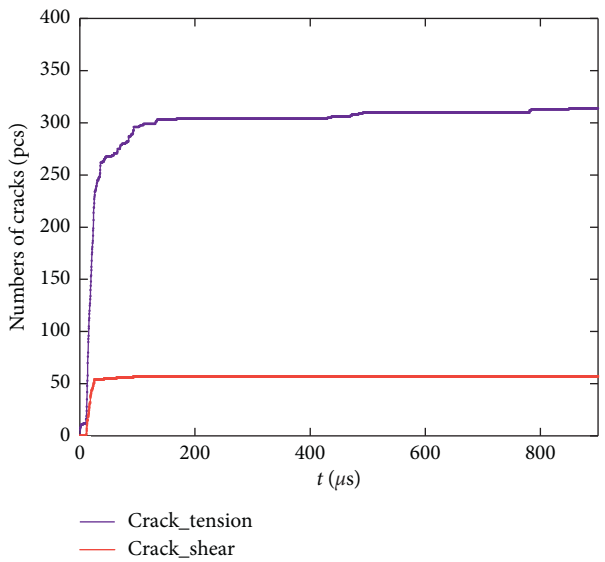

Figure 10: Cumulative numbers of tension and shear cracks with time during rock breaking.

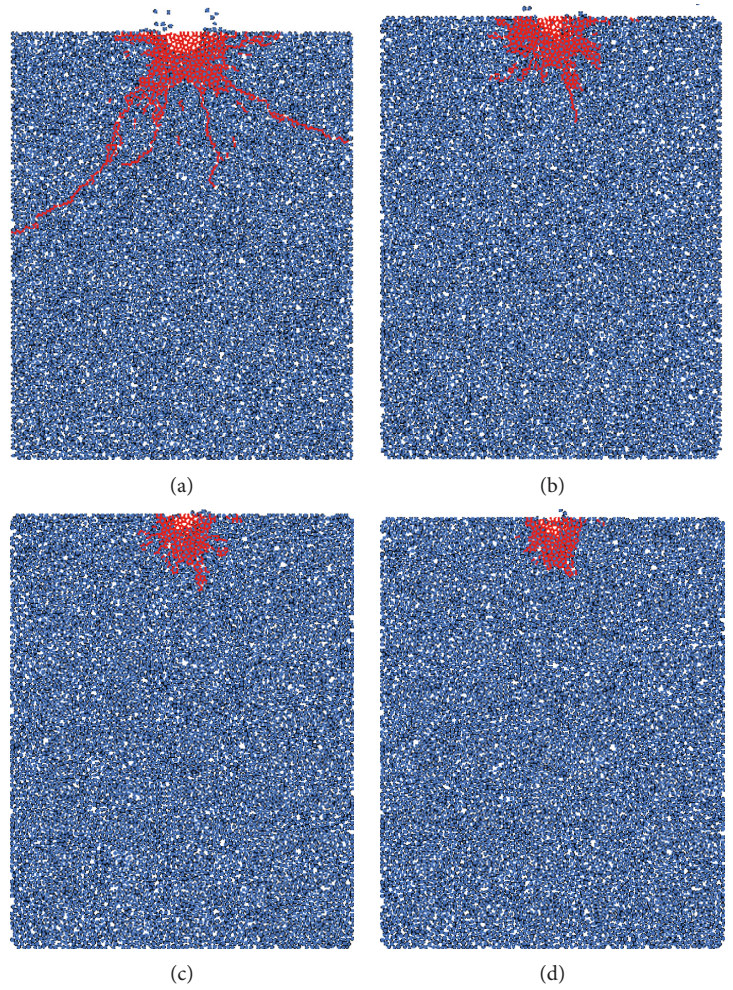

Figure 11: Breaking state of electropulses inside granite at 100 μs under confining pressures of (a) 0 MPa; (b) 12 MPa; (c) 23 MPa; and (d) 34 MPa.

Figure 10 shows a graph of the cumulative number of cracks occurring in the process of electro-pulse rock breaking at a confining pressure of 34 MPa. The probabilistic statistical distribution function of the built-in, simulated, discrete fracture network in FPC2D was used to count the number of cracks. It was judged that a tensile stress crack occurs when the shock wave stress is greater than the tensile strength of bonding between two spherical particles, while a shear stress crack occurs when the shock wave stress is greater than the shear strength of bonding between two spherical particles. It can be seen from the figure that the cracks produced by the EPB experiment were mainly tension cracks. The numbers and times of appearance of the two types of cracks were different, as were their growth trends. When $t = 11$ μs, the first shear crack began to appear. At this time, there were 19 tension cracks; then, the numbers of tension and shear cracks increased sharply. The numbers of tension and shear cracks increased steadily after 25 μs. The main reason for this phenomenon was that the tensile strength of granite was 15 MPa and the shear strength was equal to the normal stress multiplied by the tangent of the internal friction angle and the cohesion. The shear strength of granite was 54 MPa under a confining pressure equivalent to that at a depth of 3000 m. From the curve of the shock wave variation with time, we conclude that the compressive stress produced by a shock wave or stress wave within a pulse period is less than 54 MPa most of the time. Therefore, the tensile stress was the main failure mode. When the energy density was high, the values of the shock waves produced by electro-pulse rock breaking were mostly greater than the shear strength and the rock breaking energy was mainly due to the direct compressive stress wave, resulting in shear deformation. This conclusion is consistent with that of Burkin et al. [18].

Figure 11 shows the electro-pulse breaking state at 100 μs in granite under different confining pressures according to the internal damage model. The breaking height decreased with increases in confining pressure, while the impulse voltage needed to break the rock increased.

5. Conclusions

(1) A breakdown damage model of high-voltage electropulse rock breaking was established. The model was verified by comparing its results with those of experiments. The complete process of high-voltage EPB in a confining pressure environment was simulated and calculated.

(2) According to the physical parameters used in this study, the electrobreakdown field strength of granite at room temperature and pressure is 115.2 kV/cm. We conclude that this decreases with increases in the relative dielectric constant and plasma channel radius and increases with increases in elastic modulus and surface free energy. In the process of EPB, the energy in the implanted plasma channel accounts for about 30% of the total capacitance energy. After breakdown is completed, the energy utilization rate can be greatly improved by using a current source with high capacitance.

(3) According to the electrical parameters provided by the pulsed power supply, time-varying waveforms of voltage, current, power, energy, radius, and shock waves in the plasma channel were calculated by a shock wave model.

(4) According to the curves of plasma channel radius or by damage area simulation, an electrode spacing of 10 mm results in a broken-area radius of about 12 mm under atmospheric pressure. Hence, the broken area is slightly larger than the electrode spacing and drilling holes can be formed by EPB. According to the numerical results, the confining pressure loadings had a low influence on the blasting/crushing zone, while the crack length and number and breaking height were decreased by EPB. Throughout the EPB process, the main cracks were caused by tension forces.

Data Availability

The data used to support the findings of this study are available from the corresponding author upon request.

Conflicts of Interest

The authors declare that they have no conflicts of interest.

Acknowledgments

This work was supported by the National Natural Science Foundation of China (41672364 and 41602373) and the Innovation Fund of Petro-China (2016D-5007-0307).

References

[1] G. Dong and P. Chen, "A review of the evaluation, control, and application technologies for drill string vibrations and shocks in oil and gas well," *Shock and Vibration*, vol. 2016, Article ID 7418635, 34 pages, 2016.

[2] Y. Liu, Z. Guan, H. Zhang, and B. Zhang, "Development and application of the downhole drilling string shock-absorption and hydraulic supercharging device," *Shock and Vibration*, vol. 2016, Article ID 2041671, 10 pages, 2016.

[3] C. P. Li, V. Chikhotkin, and L. C. Duan, "Research progress of electro-pulse boring rock breaking technology," *Geological Science and Technology Information*, vol. 37, pp. 288–304, 2018.

[4] H. O. Schiegg, A. Rødland, G. Zhu, and D. A. Yuen, "Electro-pulse-boring (EPB): novel super-deep drilling technology for low cost electricity," *Journal of Earth Science*, vol. 26, no. 1, pp. 37–46, 2015.

[5] B. F. Lehmann, M. Reich, M. Mezzetti, E. Anders, and M. Voigt, "The future of deep drilling-A drilling system based on electro impulse technology," *Oil Gas European Magazine*, vol. 43, pp. 187–191, 2017.

[6] S. M. Razavian, B. Rezai, and M. Irannajad, "Investigation on pre-weakening and crushing of phosphate ore using high voltage electric pulses," *Advanced Powder Technology*, vol. 25, no. 6, pp. 1672–1678, 2014.

[7] M. Ito, S. Owada, T. Nishimura, and T. Ota, "Experimental study of coal liberation: electrical disintegration versus roll-crusher comminution," *International Journal of Mineral Processing*, vol. 92, no. 1-2, pp. 7–14, 2009.

[8] W. Zuo, F. Shi, K. P. van der Wielen, A. Weh, and W. Alexander, "Ore particle breakage behaviour in a pilot scale high voltage pulse machine," *Minerals Engineering*, vol. 84, pp. 64–73, 2015.

[9] M. B. He, J. B. Jiang, G. L. Huang, J. Liu, and C. Z. Li, "Disintegration of rocks based on magnetically isolated high voltage discharge," *Review of Scientific Instruments*, vol. 84, no. 2, pp. 61–70, 2013.

[10] V. I. Kurets, V. V. Lopatin, and M. D. Noskov, "Influence of local heterogeneities on discharge channel trajectory at electric pulse destruction of materials," *Journal of Mining Science*, vol. 36, no. 3, pp. 268–274, 2000.

[11] S. Boev, V. Vajov, D. Jgun et al., "Destruction of granite and concrete in water with pulse electric discharges," in *Proceedings of the IEEE International Pulsed Power Conference*, pp. 1369–1371, Columbia, MO, USA, June 1999.

[12] E. Wang, F. Shi, and E. Manlapig, "Experimental and numerical studies of selective fragmentation of mineral ores in electrical comminution," *International Journal of Mineral Processing*, vol. 112-113, pp. 30–36, 2012.

[13] S. Boev, V. Vajov, B. Levchenko et al., "Electro-pulse technology of material destruction and boring," in *Proceedings of the IEEE International Pulsed Power Conference*, pp. 220–225, Baltimore, MD, USA, July 1997.

[14] U. Andres, I. Timoshkin, J. Jirestig, and H. Stallknecht, "Liberation of valuable inclusions in ores and slags by electrical pulses," *Powder Technology*, vol. 114, no. 1–3, pp. 40–50, 2001, in Chinese.

[15] C. Li, L. Duan, S. Tan, and V. Chikhotkin, "Influences on high-voltage electro pulse boring in granite," *Energies*, vol. 11, no. 9, p. 2461, 2018.

[16] Z. C. Zhang, *Rock fragmentation by pulsed high voltage discharge and drilling equipment development*, Ph.D. thesis, Zhejiang University, Hangzhou, China, 2013, in Chinese.

[17] V. V. Burkin, N. S. Kuznetsova, and V. V. Lopatin, "Dynamics of electro burst in solids: I. Power characteristics of electro burst," *Journal of Physics D: Applied Physics*, vol. 42, no. 18, pp. 235–241, 2009.

[18] V. V. Burkin, N. S. Kuznetsova, and V. V. Lopatin, "Dynamics of electro burst in solids: II. Characteristics of wave process," *Journal of Physics D: Applied Physics*, vol. 42, no. 23, pp. 242–248, 2009.

[19] N. S. Kuznetsova, V. V. Lopatin, and A. S. Yudin, "Effect of electro-discharge circuit parameters on the destructive action of plasma channel in solid media," *Journal of Physics: Conference Series*, vol. 552, pp. 12–19, 2014.

[20] N. Kuznetsova, V. Lopatin, V. Burkin, V. Golovanevskiy, D. Zhgun, and N. Ivanov, "Theoretical and experimental investigation of electro discharge destruction of non-conducting materials," in *Proceedings of the IEEE Pulsed Power Conference*, pp. 978–984, Chicago, IL, USA, June 2011.

[21] S. H. Cho, B. Mohanty, M. Ito et al., "Dynamic fragmentation of rock by high-voltage pulses," in *Proceedings of the American Rock Mechanics Association: ARMA*, vol. 6, pp. 1118–1128, Golden, CO, USA, June 2006.

[22] S. H. Cho, S. S. Cheong, M. Yokota, and K. Kaneko, "The dynamic fracture process in rocks under high-voltage pulse fragmentation," *Rock Mechanics and Rock Engineering*, vol. 49, no. 10, pp. 3841–3853, 2016.

[23] S. H. Cho and K. Kaneko, "Influence of the applied pressure waveform on the dynamic fracture processes in rock," *International Journal of Rock Mechanics and Mining Sciences*, vol. 41, no. 5, pp. 771–784, 2004.

[24] Y. Sun, R. Fu, A. Fan, Y. Gao, and P. Yan, "Study of rock fracturing generated by pulsed discharging under confining pressure," in *Proceedings of the IEEE Pulsed Power Conference (PPC)*, pp. 1–4, Austin, TX, USA, June 2015.

[25] K. P. Van der Wielen, R. Pascoe, A. Weh, F. Wall, and G. Rollinson, "The influence of equipment settings and rock properties on high voltage breakage," *Minerals Engineering*, vol. 46-47, pp. 100–111, 2013.

[26] H. Inoue, I. V. Lisitsyn, H. Akiyama, and I. Nishizawa, "Pulsed electric breakdown and destruction of granite," *Japanese Journal of Applied Physics*, vol. 38, no. 11, pp. 6502–6505, 1999.

[27] U. Andres, I. Timoshkin, and M. Soloviev, "Energy consumption and liberation of minerals in explosive electrical breakdown of ores," *Mineral Processing and Extractive Metallurgy*, vol. 110, no. 3, pp. 149–157, 2013.

[28] J. Biela, C. Marxgut, D. Bortis, and J. Kolar, "Solid state modulator for plasma channel drilling," *IEEE Transactions on Dielectrics and Electrical Insulation*, vol. 16, no. 4, pp. 1093–1099, 2009.

[29] Q. Hu, "experimental researches on pulse plasma discharge for deep-ocean thin-layer mineral resources crushing," *Thalassas: An International Journal of Marine Sciences*, vol. 35, no. 2, pp. 1–8, 2019.

[30] I. V. Timoshkin, J. W. Mackersie, and S. J. Macgregor, "Plasma channel microhole drilling technology," in *Proceedings of the IEEE International Pulsed Power Conference*, pp. 1336–1339, Dallas, TX, USA, June 2003.

[31] B. M. Kovalchuk, A. V. Kharlov, V. A. Vizir, V. V. Kumpyak, V. B. Zorin, and V. N. Kiselev, "High-voltage pulsed generator for dynamic fragmentation of rocks," *Review of Scientific Instruments*, vol. 81, pp. 308–311, 2010.

[32] C. Li, L. Duan, S. Tan, V. Chikhotkin, and W. Fu, "Damage model and numerical experiment of high-voltage electro pulse boring in granite," *Energies*, vol. 12, no. 4, p. 727, 2019.

[33] N. Kuznetsova, V. Lopatin, V. Burkin, V. Golovanevskiy, D. Zhgun, and N. Ivanov, "Theore-tical and experimental investigation of electro discharge destruction of non-conducting materials," in *Proceedings of the IEEE Pulsed Power Conference*, pp. 267–273, Chicago, IL, USA, June 2011.

[34] J. C. Fothergill, "Filamentary electromechanical breakdown," *IEEE Transactions on Electrical Insulation*, vol. 26, no. 6, pp. 1124–1129, 1991.

[35] A. W. Hefer, A. Bhasin, and D. N. Little, "Bitumen surface energy characterization using a contact angle approach," *Journal of Materials in Civil Engineering*, vol. 18, no. 6, pp. 759–767, 2006.

[36] I. W. Mcallister, "Partial discharges in spheroidal voids," *IEEE Transactions on Dielectrics and Electrical Insulation*, vol. 4, pp. 456–461, 2002.

[37] J. L. Jiang, S. Lan, and J. X. Yang, "Numerical analysis of the plasma characteristics of pulsed discharge in water," *Journal of Harbin University of Science and Technology*, vol. 13, pp. 107–111, 2008.

[38] X. T. Zhou, T. Sheng, X. L. Leng, X. D. Fu, and Z. Cui, "Viscous artificial boundary for seismic dynamic time-history analysis with granular discrete element method and its application," *Rock Mechanics and Rock Engineering*, vol. 36, pp. 928–939, 2017, in Chinese.

[39] C. Thornton, "The conditions for failure of a face-centered cubic array of uniform rigid spheres," *Géotechnique*, vol. 29, no. 4, pp. 441–459, 1979.

[40] Y. M. Lu, "Study on strength characteristics of rock joints under pre cyclic shear," Master's thesis, Chongqing University, Chongqing, China, 2017, in Chinese.

[41] Itasca Consulting Group Inc., *PFC2D/3D (Particle Flow Code in 2/3 Dimensions) Version 3.0*, ICG, Minneapolis, MN, USA, 2004.

[42] T. Saksala, "Numerical study of the influence of hydrostatic and confining pressure on percussive drilling of hard rock," *Computers and Geotechnics*, vol. 76, pp. 120–128, 2016.

[43] A. B. Jin, J. W. Liu, Y. Q. Zhao, B. X. Wang, H. Sun, and Y. D. Wei, "Mechanical characteristics analysis of granite under unloading conditions," *Rock and Soil Mechanics*, vol. 40, no. 1, pp. 459–467, 2019.

[44] V. F. Vazhov, S. Y. Datskvich, M. Y. Zhurkov, and V. M. Muratov, "Electric pulse breakdown and rock fracture in a coupled environment of increased pressure and temperature," *Journal of Physics: Conference Series*, vol. 552, 2014.

[45] I. V. Lisitsyn, H. Inoue, I. Nishizawa, S. Katsuki, and H. Akiyama, "Breakdown and destruction of heterogeneous solid dielectrics by high voltage pulses," *Journal of Applied Physics*, vol. 84, no. 11, pp. 6262–6267, 1998.